BEARING CAPACITY OF SANDY SOIL FOR ECCENTRIC AND INCLINED LOADS AND LATERAL RESISTANCE OF SINGLE PILES EMBEDDED IN SANDY SOIL

by Tomio Shinohara[1], Tetsuro Tateishi[2]
and Koichi Kubo[1]

PART I

Bearing capacity of sandy soil for eccentric and inclined loads

INTRODUCTION

There are many cases in which foundations are subjected to eccentric and inclined loads. Especially at the time of an earthquake eccentricity and inclination of loads are likely to increase greatly.

Several theoretical methods to compute the bearing capacity for eccentric and inclined loads have been proposed; all of which, however, being based on extremely simplified conditions, are inadequate for actually designing structures with complicated factors. The conventional methods which are now in practical use for the design are as follows.

1) For the eccentricity of loads:
The maximum soil reaction is computed with the assumption of linear variation of soil reaction under eccentric loads and then is compared with the allowable bearing capacity for the concentric load.

2) For the inclination of loads:
The possibility of sliding along the bottom surface of the foundation is examined assuming no effect of the horizontal component upon the bearing capacity.

It is evident that both of the above mentioned methods are theoretically incorrect. We consequently performed an experimental study to demonstrate that even in complicated field conditions, by the computations assuming a circular sliding surface within the sand mass, the bearing capacity of sandy soil can be estimated with an accuracy sufficient for practical purposes.

COMPUTATIONS OF THE ULTIMATE BEARING CAPACITY

The following assumptions are made as the bases of our computations.

1) The sliding surfaces have the shape of a circular arc.

2) A sliding surface starts from one of the three points A, B or C as shown in Figure 1-a.

---

1. Ministry of Transportation, Japanese Government
2. Japan Steel and Tube Corporation; Formerly Ministry of Transportation, Japanese Government

The point C can be one of the possible starting points since the distribution of sand reaction to the base of the slab rapidly changes near the point C as shown in Figure 1-b causing high shearing stresses in the sand mass.

3) The magnitude of the maximum load which can be applied to the slab is computed from the conditions of the equilibrium of the soil mass in the sliding surface by means of friction circle method assuming that the soil mass moves as a solid body.

4) The lowest of the maximum loads which are computed for the three possible sliding surfaces will be the ultimate bearing capacity.

The bearing capacity in the case of the horizontal ground surface with no embedment of the slab is given by the following equation.

$$\frac{V}{2b} = N \cdot \gamma \cdot b$$

The following results are obtained from the computations.

1) From Figure 2 which shows a comparison between the ultimate bearing capacities obtained by means of the new method and the existing methods it can be concluded that the new method gives to the computations an accuracy sufficient for practical purposes.

2) The computation results when $\phi = 40^\circ$ are shown in Figure 3.

MATERIALS AND METHOD OF THE TESTS

The sketch of the apparatus used is shown in Figure 4. The following items will be worth mentioning.

1) Setting of α and e for the load:
By adjusting the relative positions of the model slab the loading frame attached to the wire and the pulley A, the arbitrary combinations of α and e were obtained.

2) Loading method:
The load was instantaneously applied by releasing an oil jack which was supporting the loading disk carrying a certain amount of weights. The loading was repeated while increasing each time the magnitude of load until it reached the failure load.

3) Sand:
Air dried fine sand was used. The dry density and the friction angle were found to be approximately 1.4 and 40°. Along the glass wall horizontal and vertical lines of white sand were placed so as to make the observations of the sliding surfaces easy.

4) Observations:
In addition to the recording of the developments of the failure surfaces by a movie camera, we took several photographs exposing them during the time of sliding to get the shape of sliding surfaces and the movement of sand particles. An example of the photographs is shown in Figure 5.

TEST RESULTS

The shape of the sliding surfaces can be devided into four cases as shown in Figure 6 depending on the combination of α and e .

1) The case of $e<0$:

The sliding surface of type A shown in Figure 1-2 develops with the backward tilting and forward movement of the slab.

2) The case of $e>0$:

The sliding surface of type C occurs and the slab tilts and moves forward. Sometimes a small and shallow sliding surface is observed near the front end of the slab when α is relatively large.

3) The case of very large e and small α :

The sliding surface of type B develops with the heavy tilting of the slab.

4) The case of small e and small α together with the case which is between case 2) and case 3):

Soil wedge somewhat like Kurdumoff wedge is observed in the soil mass and the sliding surfaces develop in both sides starting at the top of the wedge. An example of this case is shown in Figure 7.

Several tests were conducted varying the distance between the two glass walls and accordingly changing the length of the model slab. The purpose of the tests was to study effects of the frictional resistance between the walls and the soil mass in the sliding surface. The test results shown in Figure 8-a agree very well with the values which are obtained by the computation for the case of $\mu \cdot K = 0.45$ assuming the conditions shown in Figure 8-b. In the same way the frictional resistance was deducted from all of the test results in evaluating the bearing capacity coefficient N. As shown in Figures 9 to 11 the values of N thus obtained show fairly good agreement with the values which are obtained by the analytical method proposed above. The one of the sliding surfaces observed in the tests is compared with that estimated by the analitical method in Figure 12. They agree very well even though the former is a little smaller.

CONCLUSION

1. The shape of sliding surfaces and the value of the ultimate bearing capacity for the sandy soil can be estimated with an accuracy sufficient for practical purposes by assuming a circular sliding surface in the sand mass.

2. By this method the bearing capacity coefficient for various combinations of the eccentricity and the inclination of the load can be computed beforehand only if we know the property of soil and the dimmensions of the slab.

3. The complicated conditions such as inclination and irregularity of the ground surface or inhomogeneity of the soil mass can not be dealt with by conventional methods but even in such cases the ultimate bearing capacity can be very easily evaluated by the new method.

4. This method also makes it possible to compute the bearing capacity coefficient for various loading conditions at the time of an earthquake if the effects of the earthquake are taken into consideration by statically applying the seismic force to the soil mass in the sliding surface. Also the small value of the ultimate bearing capacity during earthquake because of the large amounts of α and e can be understood very easily from Figure 5.

5. The considerable settlement of the slab before the full development of the sliding surface was observed in the tests. The same kind of settlement is likely to occure in a greater degree during earthquake. Consequently, in the case of very loose sand the allowable bearing capacity seems to take a considerable low value determined by the allowable settlement rather than by the failure condition.

6. The denseness of foundation soil is also desirable especially near the front end of the slab because it prevents the occurence of a small local failure as mentioned above in the description of the test results.

7. If the settlement of soil near the front end of the slab is prevented by some means such as compaction of soil or driving of piles the distribution of the soil reaction seems to approach one represented by the broken line in Figure 1-b. Accordingly the starting point of the sliding surface is likely to move to the point A making the occurence of the sliding surface from C rather difficult and thus relatively high bearing capacity can be expected.

8. It is probable that the bearing capacity of the slab which has large dimensions is smaller than the value estimated by the computations because of the progressive failure of the soil. To take this probability into consideration it is desirable to use a smaller value of ϕ or to use a larger value of the safety factor in the computations of the allowable bearinn capacity.

PART II

Lateral resistance of single piles embedded in sandy soil

INTRODUCTION

It is needless to say that the knowledge of the lateral resistance of the piles is essential for the aseismic design of a pile foundation or a pile structure, but even the exact nature of the lateral resistance against statically applied lateral force is not entirely clear to us. It is to study the basic characteristics of this lateral resistance of piles that we performed lateral load tests on single free-head model piles embedded in sandy soil.

MATERIALS AND PROCEDURE

1. The soil property and the method of compaction:

All tests were conducted in a concrete testing tank, the length, the width and the depth of which being 8 m, 4.5 m and 4 m. The soil used was medium size river sand. The results of the grain size analysis and the triaxial tests are shown in Figures 13 and 14 respectively. After the sand was dumped in the water, eight coverages of hand tamping were performed with a 30 cm × 30 cm wooden tamper weighing 8.3 kg to create 20 cm layers. Density measurements taken after the calibrated sand method showed that the density of the compacted sand was controlled to remain 1.78 ± 0.05 gr/cm^3 for all three series of the tests.

2. Model piles:

The length and stiffness of the model piles were determined so that there might be similar deflection and earth pressure distributions between the models and the prototypes. The principal items of the model piles are given in table 1. In order to measure the bending strain, on both sides of the model piles at 11-20 levels, were attached wire strain gages, which were protected by coating the piles with cotton cloth and polyester resin. The friction angle between sand and pile surface after coating was completed was 30. The piles were then placed in the testing position in the tank, backfilled with sand and tested in saturated condition.

3. Method of loading and measurement:

The general idea of loading and measuring set-up is given in Figure.15. Horizontal load was applied to the pile head by means of calibrated weights and wire and pulley system with an increment of 1/5 - 1/10 of maximum load. All measurements were taken after the movement of the pile head had practically ceased. In the first series of the tests, two to five loops of loading were applied, each time with a maximum value doubling that of the previous loop. In the second and the third series 2 to 9 loops of the same maximum value were repeated. The measured items were 1) the deflection and the deflection angle at the pile head, 2) the magnitude of horizontal force and 3) bending strains at the surface of the pile.

4. The purposes of each siries of the tests:

The first and the second series of the tests were conducted to examine the effects of the stiffness of the pile on the lateral resistance of the pile when the height of load application was kept constant. The effects of the height of load application would be known by comparing the results of the first and the second series. The effects of the width of the pile were investigated in the third series in which all other conditions such as unit EI and pulling height were kept constant. In addition to the plate pile used in the above mentioned tests several steel pipe piles were tested to examine the effects of the shape of the pile.

TEST RESULTS

The relations between the horizontal force and the deflection at the point of load application are given in Figures 16. An example of the moment distribution curves obtained by the strain gage measurements is shown in Figure 17. The first and the second differentiations of a moment

curve give shear and pressure curves and the first and the second integrations give deflection angles and deflection respectively. The results of such calculations done graphically for the pile PP-2 are shown in Figure 17.

Figure 18 shows the effect of EI upon the distributions of moment, deflection and soil reaction. It is to be seen that the effective length of the piles increases and the deflection at the ground surface decreases, as EI increases, but EI has little effect on the magnitude of maximum moment. Examples of changes in the distributions of moment, deflection and soil reaction with the increase of the horizontal force are shown in Figure 19. In Figure 20 the maximum moment and pile deflection at the ground surface are plotted against horizontal force. It should be noted that the curves show no linear relationship.

ANALYSIS OF THE TEST RESULTS AND DISCUSSIONS

1. Coefficient of horizontal subgrade reaction.

Most of the theoretical analyses proposed for this problem made an assumption of a simple relationship between soil reaction and pile deflection to solve the following fundamental differential equation for beam.

$$EI\frac{d^4y}{dx^4} = p = f(x, y) \qquad \cdots\cdots\cdots (1)$$

And the following expressions have usually been used for f(x,y).

$$p = E_s \cdot y$$
$$p = K \cdot x \cdot y$$
$$p = K \cdot x^2 \cdot y$$

An attempt was made by us to find a more adequate expression for f(x,y) on the basis of the test results. Figure 21 presents a typical relationship between the soil reaction per unit area at several levels of embedded part of the pile and the pile deflection at the corresponding points. In Figure 22 the similar relationships are plotted together for five piles each of which having different EI values. It can be noticed that the change of EI value has little effect on the p-y relationship. Figure 23 shows the linear relationship between the depth x and the soil reaction p for the same amount of the deflection y. From Figure 24 in which p/x is plotted against y, the following expression for p can be derived.

$$p = K \cdot x \cdot y^n \qquad \cdots\cdots\cdots (2)$$

For the present test n is approximately 0.5.

Naturally there are certain limitations to the validity of equation (2). When y exceeds a certain amount the soil begins to fail and the rate of increase of p decreases very repidly. In Figure 24 it is seen that the test data deviate from the curve $p/x = K \cdot y^{0.5}$ where y is larger than 1 cm.

2. Effect of the width of the pile.

The Figures 21 to 24 represent the results of the first series of tests only but similar figures can be plotted for the second and the third series

of tests in which the height of the load application and the width of the piles were varied. Thus it may be concluded that the expression $p = K \cdot x \cdot y^{0.5}$ is valid for all conditions of the present tests except when y is too large. The constant K is scarcely effected by the change of EI and the shape of the piles, but it increases as the width decreases and the rate of increase becomes very large when the width is smaller than 10 cm. The relationship between K and the width of the pile is shown in Figure 25. Similar relationship can be seen between lateral load T and ground surface deflection y_0. The results of the third series of tests are shown in Figure 26 in which T per 10 cm width of pile is plotted against y_0 in log-log scale. From this figure the following expression is derived.

$$T = \alpha \cdot y^m \quad (m \fallingdotseq 0.7) \qquad \cdots\cdots\cdots (3)$$

The constant α is plotted against the width of the piles in Figure 27 with a correction for the different values of EI of the pipe piles. It can be concluded that for the prototype piles which usually have a width larger than 20 cm the width of the piles have practically no effect on the p-y relationship of such soil as used in the tests.

3. The application of the test results to prototype piles.

The behavior of prototype piles can be predicted from the test results on model piles by applying the law of similarity. The following conditions must be satisfied for the similarity of deflection between a model pile and a prototype pile.

$$\begin{aligned} R_{EI} &= R_q \cdot \frac{R_x^4}{R_y} \\ R_s &= R_{EI} \cdot \frac{R_y}{R_x^3} = R_q \cdot R_x \\ R_M &= R_{EI} \cdot \frac{R_y}{R_x^2} = R_q \cdot R_x^2 \end{aligned} \qquad \cdots\cdots\cdots (2)$$

Since

$$P = K \cdot x \cdot y^{0.5}$$

Then

$$q = K \cdot x \cdot y^{0.5} \cdot b \qquad \cdots\cdots\cdots (3)$$

By substituting (3) into (2) the following relationships are obtained.

$$\begin{aligned} R_y &= R_x^{10} \cdot R_{EI}^{-2} \cdot R_K^2 \cdot R_b^2 \\ R_s &= R_x^7 \cdot R_{EI}^{-1} \cdot R_K^2 \cdot R_b^2 \\ R_M &= R_x^9 \cdot R_{EI}^{-1} \cdot R_K^2 \cdot R_b^2 \end{aligned} \qquad \cdots\cdots\cdots (4)$$

The moment distributions of the piles PP-3, PP-4, and PP-5 for the loads which satisfy the similarity conditions given in (4) are compared in Figure 28. A Similar comparision is made in Figure 29 for the piles PP-1, PP-2 and PP-3. Both of these figures show very good similarity between the moment curves of the different piles.

By employing the convertion factors in (4) the T-y_0 curves for all piles tested in the first and the second series are converted into the curves for the PP-4 giving a representative curve 'D' as shown in Figure 30. From this curve 'D', T-y_0 curves for prototype piles can be obtained for any height of load application also by employing the same convertion factors. The T-y_0 curves for a timber pile and a steel H-pile thus obtained are shown in Figures 31 and 32. (A complementary test for PP-1 was conducted to examine

the case of load application at the ground surface.)

These curves, together with similar ones for the maximum moment and the effective length of piles, give sufficient data for designing a free-head pile embedded in such soil as used in the tests. To obtain design curves for different conditions of foundation soil and various types of piles another series of model tests are now being conducted by us.

SUMMARY

The new expression for the relationship between the soil reaction p and the pile deflection y was proposed. It was also shown that the behavior of prototype piles can be predicted from the test results on the model piles by applying the rule of similarity which are derived from the proposed expression for p and y.

BIBLIOGRAPHY

PART I

1. "Aseismic Design of Quay Walls in Japan" by R. Amano, H. Azuma and Y. Ishii, Proc. World Conf. on Earthquake Engineering, 1956.

2. "The Bearing Capacity of Foundation Under Eccentric and Inclined Loads" by G.G. Meyerhof, Proc. 3rd Int. Conf. on Soil Mech. and Found. Eng. 1953.

3. "Rupture Surface in Sand under Oblique Loads" by A.R. Jumikis, Proc. A.S.C.E. Vol. 82, SM-1, 1956.

PART II

4. "Lateral Pile Loading Tests" by L. B. Feagin Trans. A.S.C.E., Vol. 102, 1937.

5. "The Earth Pressure and Deflection Along the Embedded Lengths of Piles Subjected to Lateral Thrust" by L.A. Palmer and J.B Thompson, Proc. 2nd Int. Conf. on Soil Mech. and Found. Eng. 1948.

6. "Symposium on Lateral Load Tests on Piles" A.S.T.M. Special Technical Publication No. 154, No. 154-A 1953, 1954.

7. "The Single Pile Subject to Horizontal Force" by P.W. Rowe, Geotechnique, Vol. 6, No.2, 1956.

8. "Evaluation of Coefficient of Subgrade Reaction" by K. Terzaghi, Geotechnique, Vol. 5, No.4, 1955.

9. "Soil Modulus for laterally Loaded Piles" by B. McClelland and J. A. Focht, Jr., Proc. A.S.C.E. Vol. 82, SM-4, 1956.

NOMENCLATURE

Part I

V	:	Vertical component of inclined load
2b	:	Width of the slab
N	:	Bearing capacity coefficient
γ	:	Unit weight of sand
ϕ	:	Friction angle of sand
α	:	Ratio of horizontal component to vertical component of the load
e	:	Eccentricity (see Fig. 1-a)
μ	:	Friction angle between sand and glass wall
K	:	Coefficient of earth pressure (see Fig. 8-b)

PartII

p	:	Net sorl reaction per unit area of the pile surface
x	:	Depth below the ground surface
y	:	Pile deflection
y_0	:	Pile deflection at the ground surface
E	:	Modulus of elasticity of the Pile
m, n	:	Parameter
K, Es, α'	:	Coefficients
R	:	Ratio between corresponding factors of model and prototype
q	:	Soil reaction per unit length of the pile
T	:	Total horizontal load

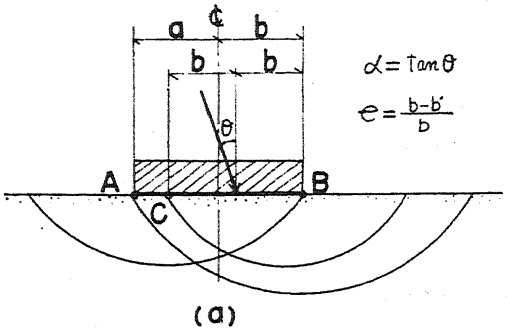

Fig. 1-a Three types of sliding surface

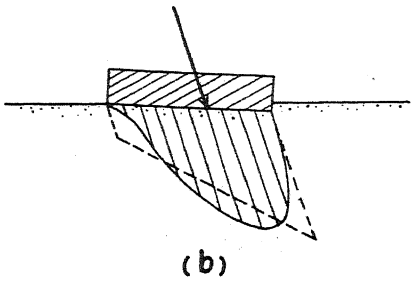

Fig. 1-b Distrubution of soil reaction under the loading slab

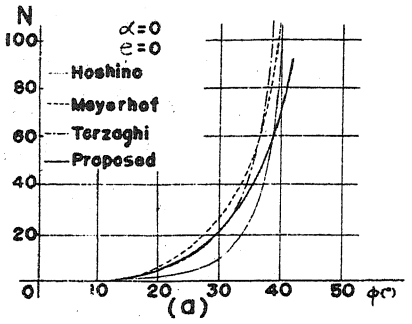

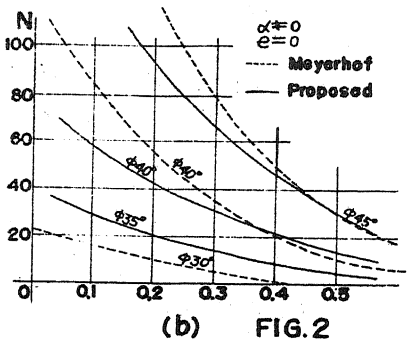

Fig. 2 Comparison of bearing capacity coefficients computed by various methods

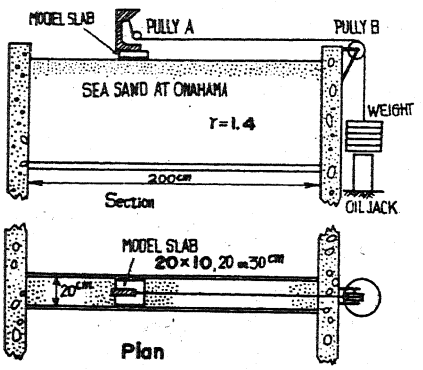

Fig. 4 Sketch of the testing apparatus

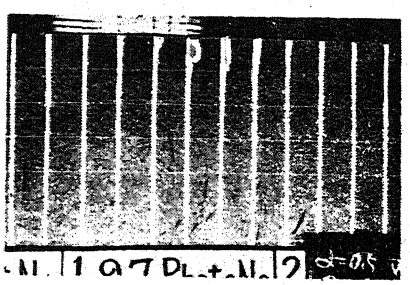

Fig. 5 An example of photographs showing the sliding surface in the soil mass

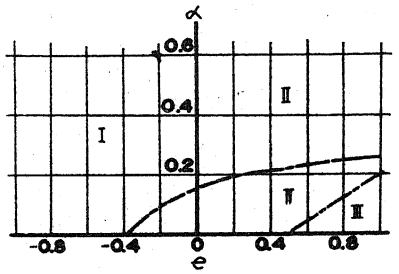

Fig. 6 Classification of failure patterns by combination of α and e

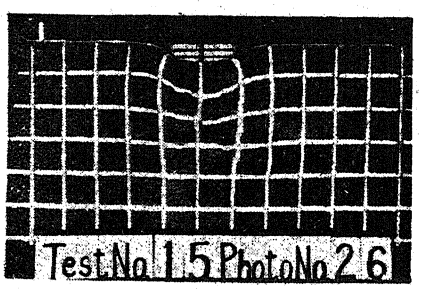

Fig. 7 Same with Fig. 5

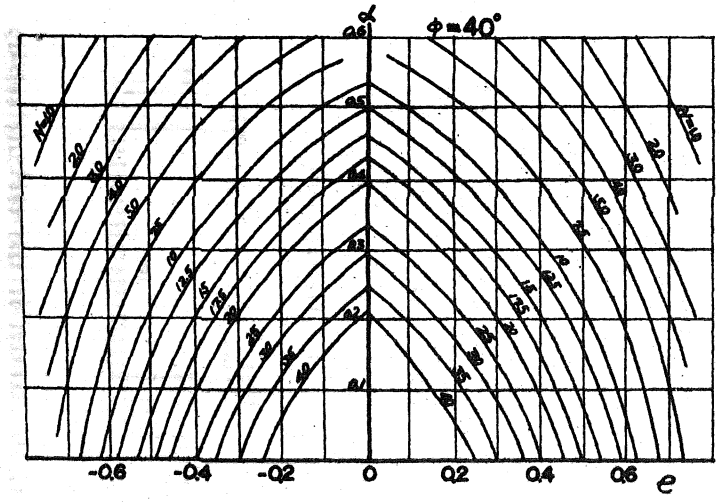

Fig. 3 Bearing capacity coefficient for the case of of ϕ = 40° computed by the proposed method

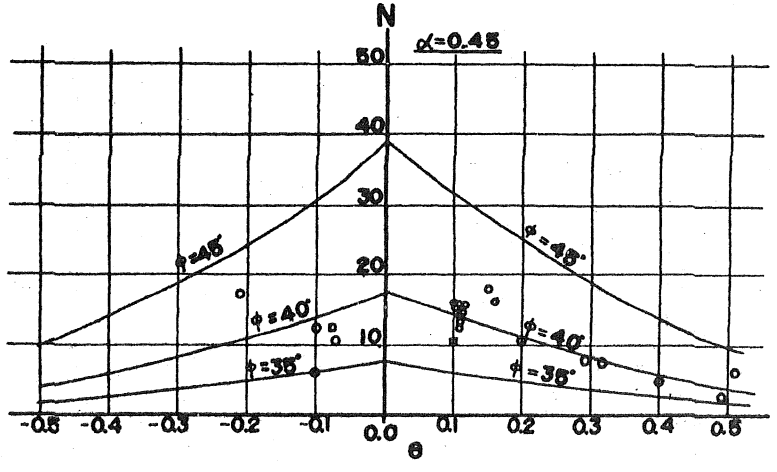

Fig. 9 Comparison between measured and computed bearing capacity coefficients

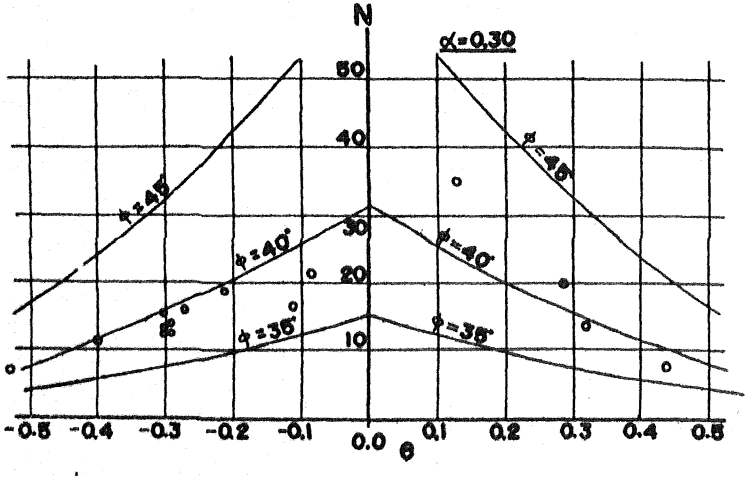

Fig. 10 Comparison between measured and computed bearing capacity coefficients

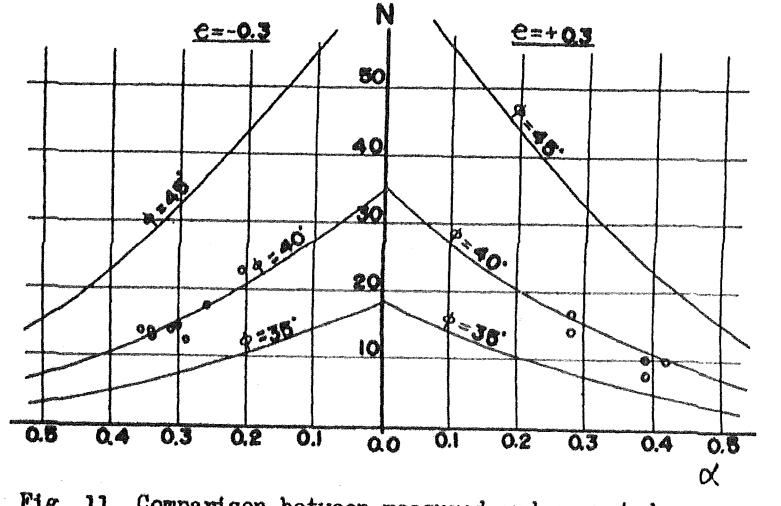

Fig. 11 Comparison between measured and computed bearing capacity coefficients

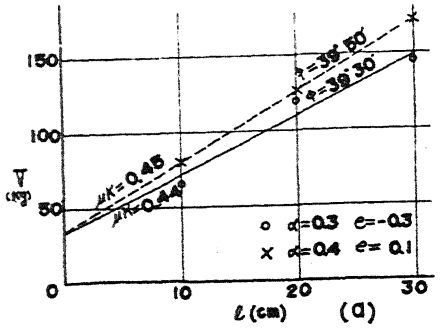

Fig. 8a Results of the tests on the side friction

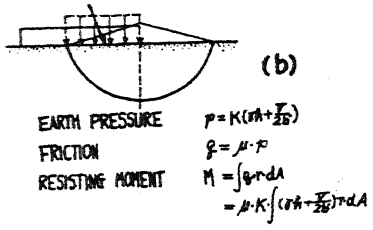

Fig. 8b Computation method of the side friction

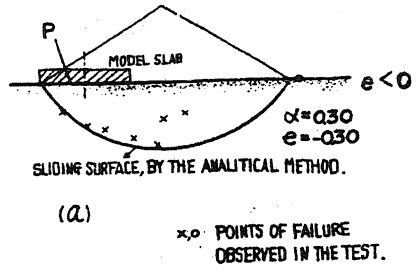

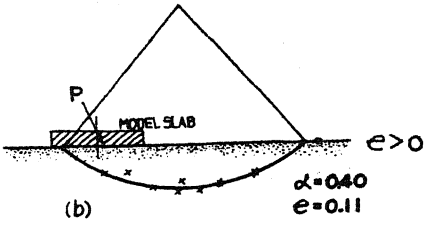

Fig. 12 Comparison between obserbed and computed sliding surfaces

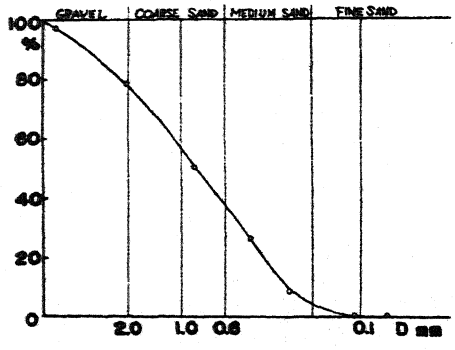

Fig. 13 Grain size distribution curve

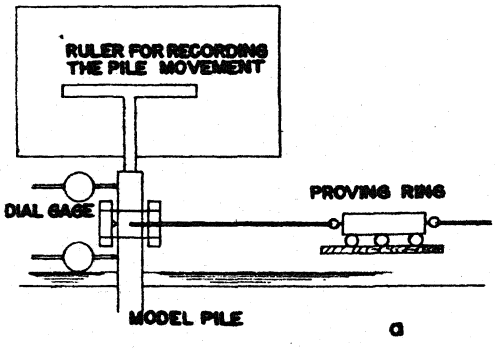

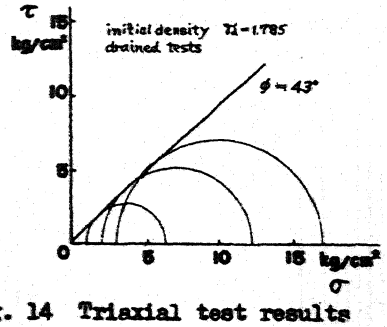

Fig. 14 Triaxial test results

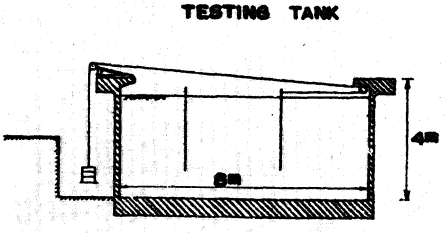

Fig. 15 Sketch of the testing set-up

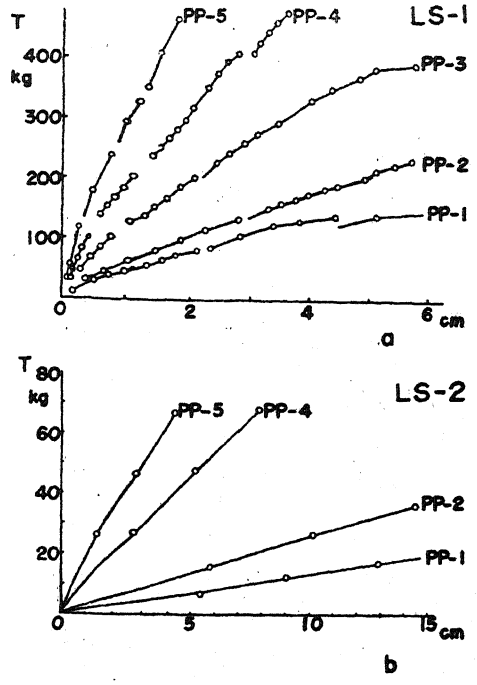

Fig. 16 Load deflection curves at the pile heads

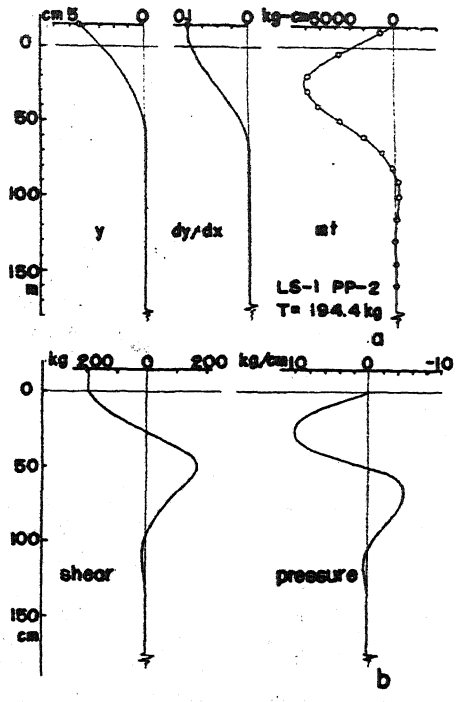

Fig. 17 Distribution of Mt, Shear, Pressure, dy/dx and y for the pile PP-2

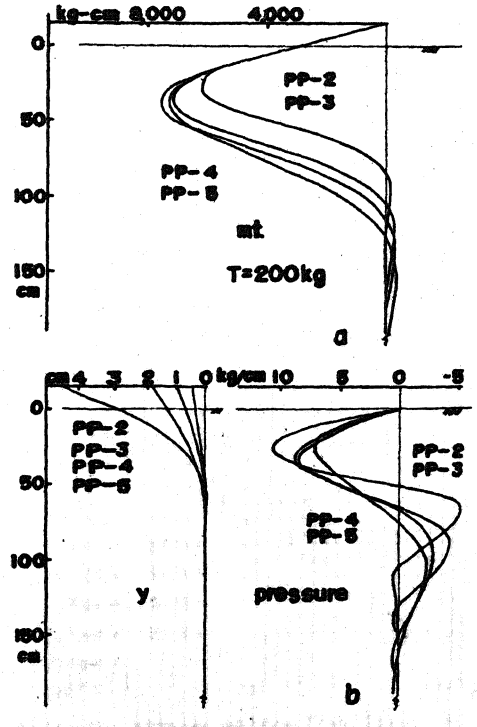

Fig. 18 Effect of EI

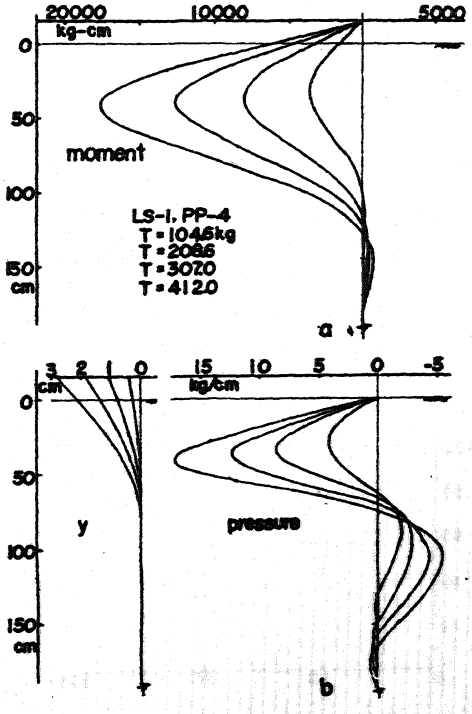

Fig. 19 Effect of Magnitude of lateral load

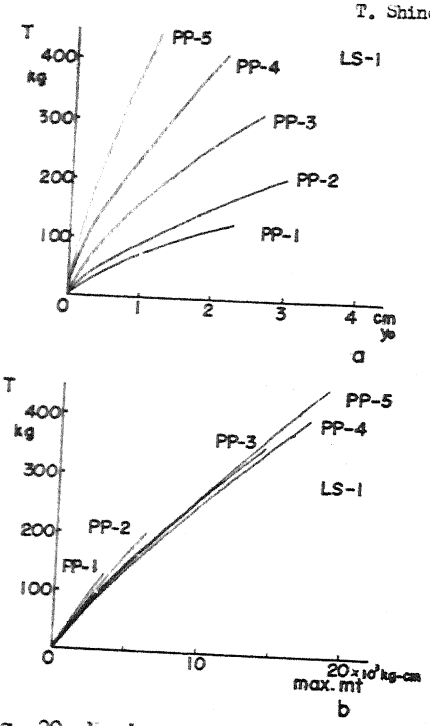

Fig. 20 Maximum moment and ground surface deflection plotted against lateral load

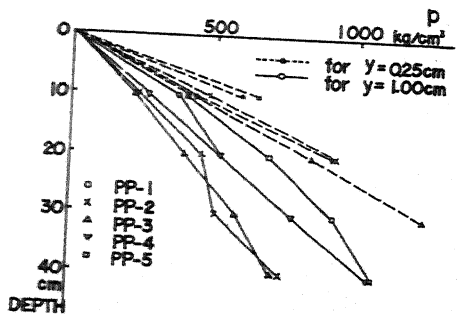

Fig. 23 Relations between depth x and soil reaction p

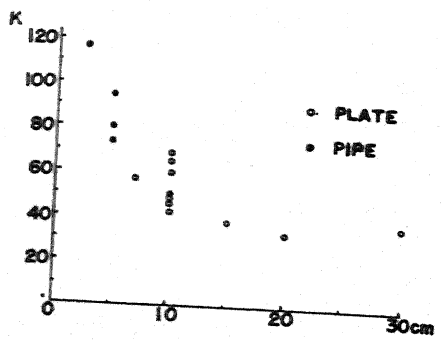

Fig. 25 Effect of pile width on the coefficient K

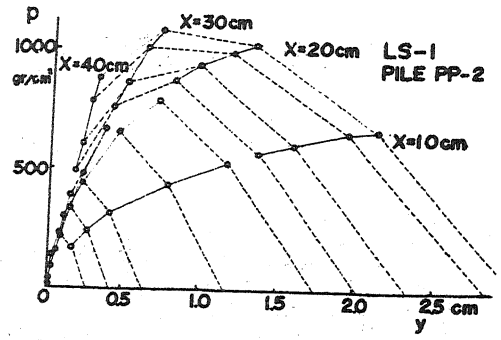

Fig. 21 p-y relationship for the pile PP-2

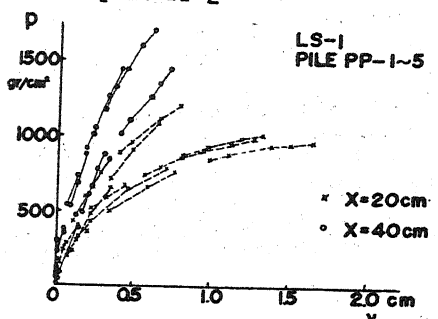

Fig. 22 p-y relationships at the levels of 20 cm and 40 cm

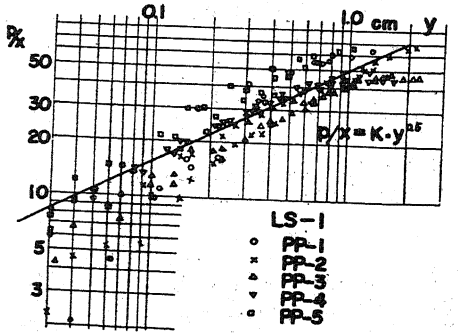

Fig. 24 p/x - y relationship plotted in logarithmic scale

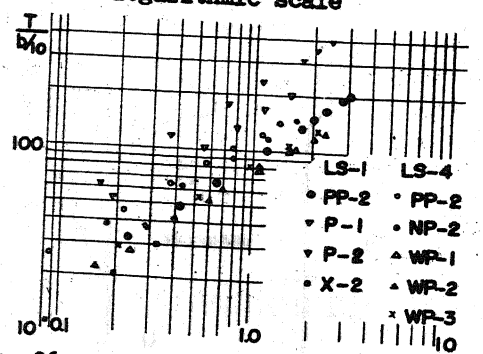

Fig. 26 Load deflection curves plotted in logarithmic scale

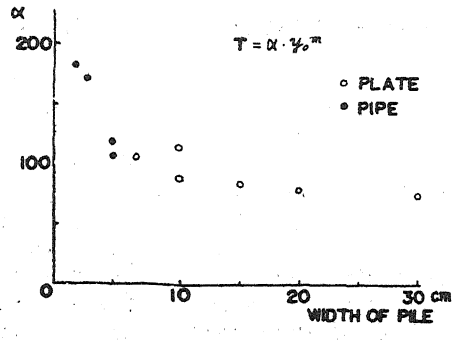

Fig. 27 Effect of pile width on the coefficient α

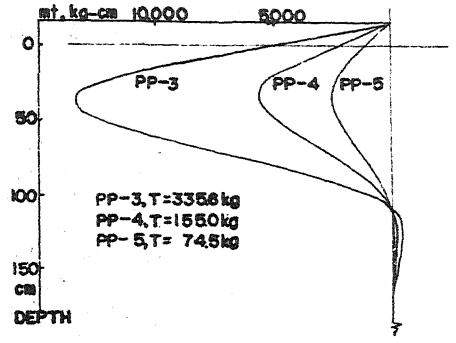

Fig. 28 Comparison of moment distributions (PP-3, PP-4 and PP-5)

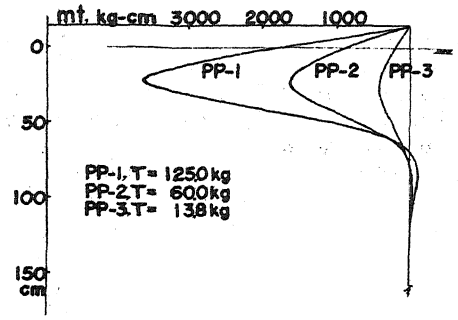

Fig. 29 Comparison of moment distributions (PP-1, PP-2 and PP-3)

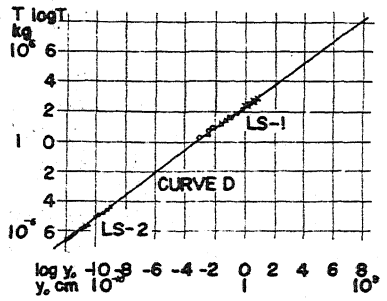

Fig. 30 Representative curve "D" for PP-4

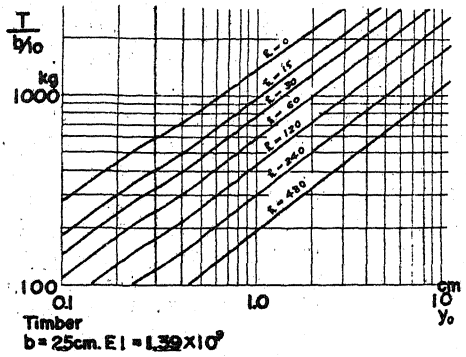

Fig. 31 Load deflection curves for a timber pile

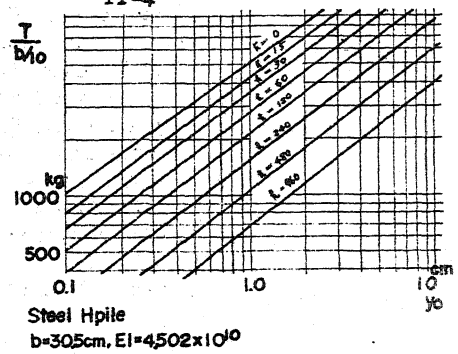

Fig. 32 Load deflection curves for a Steel H-pile

TABLE-1

1st Series, LS-1

Pile	Bcm	lcm	hcm	EI kg - cm²	type
PP-1	10	240	15	1.408 × 10⁶	Plate
PP-2	"	"	"	3.147 "	"
PP-3	"	"	"	12.73 "	"
PP-4	"	"	"	27.54 "	"
PP-5	"	"	"	57.34 "	"
P-1	5.08	"	"	13.44 "	Pipe
P-2	"	"	"	20.75 "	"

2nd Series, LS-2

PP-1	10	140	117	1.408 × 10⁶	Plate
PP-2	"	"	"	3.147 "	"
PP-3	"	"	"	12.73 "	"
PP-4	"	"	"	27.54 "	"
X-1	1.75	"	15	0.322 "	Pipe
X-2	2.70	"	15	1.747 "	"

3rd Series, LS-4

WP-1	30	140	15	9.070 × 10⁶	Plate
WP-2	20	"	"	5.942 "	"
WP-3	15	"	"	4.598 "	"
PP-2	10	"	"	3.166 "	"
NP-2	7	"	"	2.117 "	"
X-5	10.16	"	"	214.0 "	Pipe
X-6	5.08	"	"	34.1 "	"
PP-1	10	200	0	1.408 "	Plate

b: Width of pile, l: embedd length of pile
h: Hight of load application